

QCD-based charge symmetry breaking interaction and the Okamoto-Nolen-Schiffer anomaly

Hiroyuki Sagawa (佐川弘幸)^{1,2} Tomoya Naito (内藤智也)^{3,4}
Xavier Roca-Maza^{5,6,7} and Tetsuo Hatsuda (初田哲男)³

¹*RIKEN Nishina Center for Accelerator-based Science, Wako 351-0198, Japan*

²*Center for Mathematics and Physics, University of Aizu, Aizu-Wakamatsu, Fukushima 965-8560, Japan*

³*RIKEN Interdisciplinary Theoretical and Mathematical Sciences Program (iTHEMS), Wako 351-0198, Japan*

⁴*Department of Physics, Graduate School of Science,*

The University of Tokyo, Tokyo 113-0033, Japan

⁵*Departament de Física Quàntica i Astrofísica and Institut de Ciències del Cosmos,*

Universitat de Barcelona, Martí i Franqués 1, 08028 Barcelona, Spain

⁶*Dipartimento di Fisica, Università degli Studi di Milano, Via Celoria 16, 20133 Milano, Italy*

⁷*INFN, Sezione di Milano, Via Celoria 16, 20133 Milano, Italy*

(Dated: January 26, 2024)

An approach is proposed to link the charge symmetry breaking (CSB) nuclear interaction and the low-energy constants in quantum chromodynamics (QCD) by matching the CSB effect in nuclear matter. The resulting CSB interaction is applied to study the Okamoto-Nolen-Schiffer anomaly, still lacking a satisfactory microscopic understanding, on the energy differences of mirror nuclei by taking ^{17}F - ^{17}O , ^{15}O - ^{15}N , ^{41}Sc - ^{41}Ca , and ^{39}Ca - ^{39}K as typical examples. The magnitude and sign of the QCD-based CSB interactions are found to resolve the anomaly successfully within theoretical uncertainties.

An anomaly in the energy differences of mirror nuclei and isobaric analog states, not yet well understood from a microscopic point of view, was found more than 50 years ago and is called the Okamoto-Nolen-Schiffer (ONS) anomaly [1, 2]. It was first reported by Okamoto for the ^3He - ^3H system, and Nolen and Schiffer made a systematic study from light to heavy nuclei within the framework of the independent-particle model to find that the theoretical values of the energy difference underestimate the experimental values by 3–9%. Extra corrections such as the finite proton size, the center-of-mass effect, the Thomas-Ehrman effect, the isospin impurity, the electromagnetic spin-orbit interaction, the proton-neutron mass difference in the kinetic energy, the core polarization effect, and the vacuum polarization, altogether explain only about 1% of the discrepancy [3].

A possible remaining source to fill the gap is the charge symmetry breaking (CSB) nuclear interaction [1, 4–7]. Recently, phenomenological CSB interactions (often taken to be a Skyrme-type contact interaction) have been introduced to systematically calculate the isospin symmetry breaking effect on top of the Coulomb interaction; they provide successful results for describing the isobaric analog states, the mass differences of iso-doublet and iso-triplet nuclei, and also the double- β decays [8–14]. However, both the magnitude and the sign of the parameters in phenomenological CSB interactions have not been well determined. Meanwhile, microscopic calculations of observables sensitive to isospin symmetry breaking terms in the nuclear Hamiltonian have also become available [15] although CSB effects have not been isolated in detail.

The aim of this Letter is to provide a quantum chromodynamics (QCD)-based understanding of CSB by making

a quantitative link between the Skyrme-type CSB interactions [10, 16] and the CSB effect due to the u - d quark mass difference in QCD [17–19]. First, we perform a matching of the phenomenological and QCD-based calculations on the binding-energy difference between the neutron and the proton in an infinite nuclear matter to constrain the sign and magnitude of the phenomenological CSB interactions. Then, the results are utilized to study the mass difference of mirror nuclei ΔE of $(N \pm 1, Z)$ and $(N, Z \pm 1)$ with the closed-shell core ($A = N + Z = 16$ and 40) based on the Hartree-Fock (HF) wave functions, aiming to see whether the ONS anomaly can be resolved microscopically. These examples are chosen to suitably isolate CSB effects with respect to those originating from charge independence breaking (CIB) and, thus, robustly test our approach.

Let us start with the binding-energy difference between the neutron and the proton $\Delta_{np}(\rho)$ in infinite nuclear matter ($N = Z$) with the baryon density ρ , as defined by a difference of the momentum independent part of the Lorentz-scalar self-energies. In the leading order of the u - d quark mass difference and the quantum electrodynamics (QED) effect, an approximate formula has been obtained from the QCD sum rules (QSR) [18]:

$$\Delta_{np}(\rho) \simeq C_1 G(\rho) - C_2, \quad (1a)$$

$$G(\rho) = \left(\frac{\langle \bar{q}q \rangle}{\langle \bar{q}q \rangle_0} \right)^{1/3}. \quad (1b)$$

Here, $\langle \bar{q}q \rangle$ and $\langle \bar{q}q \rangle_0$ are, respectively, the isospin averaged in-medium and in-vacuum chiral condensate. The coefficient C_1 is proportional to the u - d quark mass

difference δm ,¹ through the isospin-breaking constant $\gamma \equiv \langle \bar{d}d \rangle_0 / \langle \bar{u}u \rangle_0 - 1$ as $C_1 = -a\gamma$ with a positive numerical constant a determined by the Borel QSR method [18]. On the other hand, C_2 is a constant originating both from δm and the QED effect, and is written as $C_2 = C_1 - \Delta_{np}(0)$, where experimental neutron-proton mass difference in the vacuum is denoted by $\Delta_{np}(0) = m_n - m_p \simeq 1.29$ MeV. Equation (1) is valid at low density $\rho < \rho_0 = 0.17 \text{ fm}^{-3}$ where the dimension-3 chiral condensate gives a dominant contribution in the operator product expansion in QSR. In the following, we take $C_1 = 5.24_{-1.21}^{+2.48}$ MeV, where the central value is obtained from $\gamma = -7.8 \times 10^{-3}$ [18] and the uncertainty is estimated from $\gamma = -(6-11.5) \times 10^{-3}$ [21]. Since the C_2 -term is density independent, it is canceled out in the following analysis.

Equation (1) implies that $\Delta_{np}(\rho)$ tends to decrease in the nuclear medium associated with the partial restoration of chiral symmetry $G(\rho) < 1$. The in-medium chiral condensate in the leading order with the Fermi-motion correction has a universal form [22, 23]

$$\frac{\langle \bar{q}q \rangle}{\langle \bar{q}q \rangle_0} \simeq 1 + k_1 \frac{\rho}{\rho_0} + k_2 \left(\frac{\rho}{\rho_0} \right)^{5/3}, \quad (2a)$$

$$k_1 = -\frac{\sigma_{\pi N} \rho_0}{f_\pi^2 m_\pi^2} < 0, \quad k_2 = -k_1 \frac{3k_{\text{F}0}^2}{10m_N^2} > 0, \quad (2b)$$

where $\sigma_{\pi N}$ is the π - N sigma term, m_π (m_N) is the pion (nucleon) mass, and f_π is the pion decay constant. The Fermi-momentum of the symmetric nuclear matter at saturation is denoted by $k_{\text{F}0} = (3\pi^2 \rho_0/2)^{1/3} = 268$ MeV. Systematic calculations using the in-medium chiral perturbation theory shows that the full chiral corrections up to next-to-next-to leading order over Eq. (2) is numerically small for $\rho < \rho_0$ [24] (see Fig. S.1 in Supplemental Material [25]). Alternative evaluation of the higher-order chiral corrections with the Δ -excitation [26] does not change this conclusion (see Fig. S.2 in Supplemental Material [25]). We note however that the values of $\sigma_{\pi N}$ have large uncertainty: On the basis of the present values of $\sigma_{\pi N}$ from the scattering data and the lattice QCD data ($N_f = 2$ and $2+1$) summarized in Fig. 47 of the FLAG Review 2021 [20], we employ a conservative estimation, $\sigma_{\pi N} = 45 \pm 15$ MeV. This value and the error happen to be similar to the old estimation in Ref. [27]. Corresponding values of $k_{1,2}$ are summarized in Table I. We note that the recent data from the pionic atoms [28] indicate that $\langle \bar{q}q \rangle / \langle \bar{q}q \rangle_0 (\rho = 0.58\rho_0) = 0.77 \pm 0.02$ which is consistent with the value obtained from Eqs. (2a) and (2b).

We decompose the mass difference between mirror nuclei $\Delta E = E(Z+1, N) - E(Z, N+1)$ into the Coulomb

TABLE I. The parameters k_1 and k_2 in Eq. (2) corresponding to the adopted $\sigma_{\pi N}$ value with $m_\pi = 135$ MeV, $m_N = 938$ MeV, and $f_\pi = 92.4$ MeV.

$\sigma_{\pi N}$ (MeV)	k_1	k_2
45 ± 15	-0.38 ± 0.13	0.0093 ± 0.0031

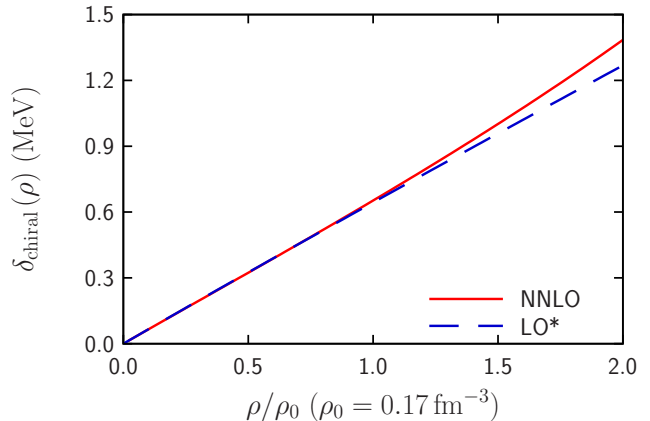


FIG. 1. The CSB effect from the partial restoration of chiral symmetry. Blue dashed curve (LO*): the leading-order formula with Fermi-motion correction [Eq. (2)]. Red curve: the NNLO result from in-medium chiral perturbation [24]. The central values of C_1 and $\sigma_{\pi N}$ are taken for these curves.

HF contribution ΔE_C and the ONS anomaly δ_{ONS} as

$$\Delta E = \Delta E_C + \delta_{\text{ONS}}. \quad (3)$$

On the basis of Eq. (1), the CSB effect to δ_{ONS} from the partial restoration of chiral symmetry in the uniform and symmetric ($N = Z$) nuclear matter δ_{chiral} can be estimated as [18]

$$\delta_{\text{chiral}} \equiv \Delta_{np}(0) - \Delta_{np}(\rho) = C_1 [1 - G(\rho)]. \quad (4)$$

Shown in Fig. 1 is δ_{chiral} as a function of the baryon density by taking the central values of C_1 and $\sigma_{\pi N}$ mentioned above. Two curves correspond to the LO result with the Fermi-motion correction (LO*) in Eq. (2) and the next-to-next-to-leading order (NNLO) result from the in-medium chiral perturbation [24]. The figure shows that Eq. (2) is quite accurate at least up to $\rho/\rho_0 \lesssim 1$. It should be noted here that δ_{chiral} is around a few hundreds keV for $\rho < \rho_0$, which is the right sign and magnitude to explain the ONS anomaly in finite nuclei.

Let us make an alternative evaluation of δ_{ONS} in Eq. (3) on the basis of the CSB interaction of an energy density functional (EDF). First of all, the general form of $E(Z, N)$ for uniform nuclear matter up to the second order of $\beta = (N - Z)/A$ reads [14]

$$\frac{E}{A} \simeq \varepsilon_0(\rho) + \varepsilon_1(\rho)\beta + \varepsilon_2(\rho)\beta^2. \quad (5)$$

¹ The renormalization group invariant mass difference reads $\delta m \equiv m_d - m_u \simeq 3.6$ MeV [20].

In particular, for $N = Z$, we find the $\Delta E|_{N=Z} = -2\varepsilon_1(\rho)$ where the effect of ε_0 and ε_2 disappears. Note that ε_1 is a genuinely CSB-type term coming only from the CSB EDF. In this Letter, we take the Skyrme-type CSB interaction [10] to evaluate its contribution to $\varepsilon_1(\rho)$:

$$V_{\text{CSB}}(\mathbf{r}) = \left[s_0(1 + y_0 P_\sigma) \delta(\mathbf{r}) + \frac{s_1}{2}(1 + y_1 P_\sigma) (\mathbf{k}^{\dagger 2} \delta(\mathbf{r}) + \delta(\mathbf{r}) \mathbf{k}^2) + s_2(1 + y_2 P_\sigma) \mathbf{k}^{\dagger} \cdot \delta(\mathbf{r}) \mathbf{k} \right] \frac{\tau_{1z} + \tau_{2z}}{4}, \quad (6)$$

where $\tau_{iz} = +1$ (-1) for neutrons (protons) is the z direction of isospin operator of nucleon i , $\mathbf{k} = (\nabla_1 - \nabla_2)/2i$, $\mathbf{r} = \mathbf{r}_1 - \mathbf{r}_2$, and $P_\sigma = (1 + \boldsymbol{\sigma}_1 \cdot \boldsymbol{\sigma}_2)/2$ is the spin-exchange operator. In Eq. (6), s_0 and y_0 are the strength parameters of the contact CSB and its spin exchange interactions, while s_1 (s_2) and y_1 (y_2) are the parameters of the momentum dependent s -wave (p -wave) CSB and its spin exchange interactions, respectively. Equation (6) gives contributions to $\varepsilon_1(\rho)$ and hence δ_{ONS} as [14]

$$\delta_{\text{Skyrme}} = -\frac{\tilde{s}_0}{4} \rho - \frac{1}{10} \left(\frac{3\pi^2}{2} \right)^{2/3} (\tilde{s}_1 + 3\tilde{s}_2) \rho^{5/3}, \quad (7)$$

where we have defined the effective coupling strengths,

$$\tilde{s}_0 \equiv s_0(1 - y_0), \quad \tilde{s}_1 \equiv s_1(1 - y_1), \quad \tilde{s}_2 \equiv s_2(1 + y_2). \quad (8)$$

Note that the Thomas-Fermi approximation is adopted to evaluate the kinetic energy terms in Eq. (5).

There have been attempts to extract $\tilde{s}_{0,1,2}$ by using various experimental data such as the energy of isobaric analog states (IAS) [8] and the mass differences of mirror and isotriplet nuclei [11]. The value of \tilde{s}_0 estimated from IAS in ^{208}Pb is $\tilde{s}_0 = -52.6 \pm 1.4 \text{ MeV fm}^3$, while the mass differences of mirror nuclei lead to two estimates; $(\tilde{s}_0, \tilde{s}_{1,2}) = (-29.2 \pm 1.2 \text{ MeV fm}^3, 0)$ and $(\tilde{s}_0, \tilde{s}_1, \tilde{s}_2) = (44 \pm 8 \text{ MeV fm}^3, -56 \pm 16 \text{ MeV fm}^5, -31.2 \pm 3.2 \text{ MeV fm}^5)$. The parameters in Ref. [11] are related to ours as $t_{0,1,2}^{\text{III}} = \tilde{s}_{0,1,2}/4$. Since the contributions of \tilde{s}_0 and $\tilde{s}_{1,2}$ tend to cancel each other in physical observables, it is rather difficult to determine the magnitude and the sign of each term only from the present experimental data.

On the other hand, our approach is to constrain $\tilde{s}_{0,1,2}$ from the low-energy constants in QCD, γ and $\sigma_{\pi N}$, by matching $\delta_{\text{Skyrme}}(\rho)$ in Eq. (7) and $\delta_{\text{chiral}}(\rho)$ expanded up to $\mathcal{O}(\rho^{5/3})$ at low densities. Then, we obtain

$$\tilde{s}_0 = -\frac{4 C_1 \sigma_{\pi N}}{3 f_\pi^2 m_\pi^2}, \quad \tilde{s}_1 + 3\tilde{s}_2 = \frac{1}{m_N^2} \frac{C_1 \sigma_{\pi N}}{f_\pi^2 m_\pi^2}. \quad (9)$$

The magnitudes and signs of \tilde{s}_0 and $\tilde{s}_1 + 3\tilde{s}_2$ are summarized in Table II, where the linear uncertainty estimation is used. To evaluate the CSB effect in finite nuclei,

where \tilde{s}_1 and \tilde{s}_2 contribute independently, two characteristic parameter sets (Cases I and II) are introduced.

To carry out precise calculation of the mass differences of mirror nuclei, we consider two types of the Skyrme EDFs for the isospin symmetric part, SGII [32] and SAMi [33]; they reproduce well, within 0.3%, the experimental radii of the $N = Z$ closed shell nuclei, ^{16}O and ^{40}Ca , as shown in Table III. It is important for any adopted EDF to reproduce the charge radii since the Coulomb energy part ΔE_C is essentially determined by the charge distribution: The change of 1% in the charge radius of ^{40}Ca gives rise to 20–30 keV difference in ΔE_C of mirror nuclei.

The contributions of the CSB interactions to the mass difference between mirror nuclei of $(N \pm 1, Z)$ and $(N, Z \pm 1)$ with the closed-shell core $A = N + Z = 16$ and 40 are calculated by using HF wave functions for SGII and SAMi. As we can see from the Table IV, \tilde{s}_0 provides a dominant contribution (210–320 keV), more than one order of magnitude larger than the $\tilde{s}_{1,2}$ contributions. The net results are slightly different from the sum of \tilde{s}_0 and $\tilde{s}_{1(2)}$ contributions due to the nonlinear effect in the calculation using EDFs. The final results of Case I and those of Case II are essentially identical due to the \tilde{s}_0 dominance, so that we focus on Case I below.

Let us now turn to the comparison of the theoretical values with our CSB interaction with the experimental mass difference of the mirror nuclei by including ΔE_C and other extra contributions [6, 8, 34, 35] (see Supplemental Material [25]). The results are summarized in Table V for SGII and Table VI for SAMi assuming Case I. First, we note that the core density and the wave function of valence orbital are calculated with the closed shell core configuration without the core polarization effect of the valence nucleon. The direct and exchange contributions of the Coulomb interaction (ΔE_D and ΔE_E with $\Delta E_C = \Delta E_D + \Delta E_E$) are obtained with the exact treatment of the exchange term. The sum of extra contributions including the finite-size effect of nucleon, the center-of-mass effect on nuclear density, the Thomas-Ehrman effect δ_{NN}^1 , the isospin impurity δ_{NN}^2 , the electromag-

TABLE II. Parameters of the Skyrme-type CSB interactions constrained from the low-energy constants in QCD. To evaluate the CSB effect in finite nuclei, where \tilde{s}_1 and \tilde{s}_2 contribute independently, two characteristic parameter sets (Cases I and II) are introduced.

	Case I	Case II
\tilde{s}_0 (MeV fm ³)	$-15.5^{+8.8}_{-12.5}$	
$\tilde{s}_1 + 3\tilde{s}_2$ (MeV fm ⁵)	$0.52^{+0.42}_{-0.29}$	
\tilde{s}_0 (MeV fm ³)	$-15.5^{+8.8}_{-12.5}$	$-15.5^{+8.8}_{-12.5}$
\tilde{s}_1 (MeV fm ⁵)	$0.52^{+0.42}_{-0.29}$	0.00
\tilde{s}_2 (MeV fm ⁵)	0.00	$0.18^{+0.14}_{-0.10}$

TABLE III. The neutron radii, the proton ones, and the charge ones of ^{16}O and ^{40}Ca . Two types of Skyrme EDFs SGII and SAMi, are adopted for the HF calculation. Experimental data are taken from Refs. [29–31].

^{16}O			
	r_n	r_p	r_c
SGII	2.601	2.626	2.744
SAMi	2.625	2.648	2.765
Expt. [29]	—	—	2.737
^{40}Ca			
	r_n	r_p	r_c
SGII	3.325	3.374	3.467
SAMi	3.342	3.390	3.482
Expt. [30]	3.375	3.385	3.480
Expt. [31]	—	—	3.478

TABLE IV. Contributions from the Skyrme CSB interactions to δ_{ONS} in Cases I and II with theoretical uncertainties. The values are given in unit of keV. The core density and the wave function of valence orbit are calculated by HF model with Skyrme EDFs, SGII and SAMi. All the values are obtained self-consistently.

	Nuclei	$^{17}\text{F-}^{17}\text{O}$	$^{15}\text{O-}^{15}\text{N}$	$^{41}\text{Sc-}^{41}\text{Ca}$	$^{39}\text{Ca-}^{39}\text{K}$
	Orbital	$1d_{5/2}$	$(1p_{1/2})^{-1}$	$1f_{7/2}$	$(1d_{3/2})^{-1}$
SGII	\tilde{s}_0	229^{+192}_{-125}	269^{+221}_{-148}	292^{+245}_{-160}	322^{+264}_{-176}
	\tilde{s}_1 ($\tilde{s}_2 = 0$)	$-5.0^{+2.8}_{-4.0}$	$-5.6^{+3.1}_{-4.5}$	$-6.6^{+3.7}_{-5.3}$	$-6.0^{+3.4}_{-4.9}$
	\tilde{s}_2 ($\tilde{s}_1 = 0$)	$-6.4^{+3.5}_{-5.2}$	$-3.3^{+1.8}_{-2.7}$	$-5.3^{+2.9}_{-4.3}$	$-5.0^{+2.8}_{-4.1}$
	Case I	224^{+192}_{-125}	264^{+221}_{-148}	287^{+245}_{-160}	315^{+264}_{-176}
	Case II	225^{+192}_{-125}	266^{+221}_{-148}	289^{+245}_{-160}	316^{+264}_{-176}
	SAMi	\tilde{s}_0	211^{+174}_{-115}	274^{+225}_{-152}	278^{+230}_{-151}
\tilde{s}_1 ($\tilde{s}_2 = 0$)		$-5.2^{+2.9}_{-4.2}$	$-5.4^{+3.0}_{-4.4}$	$-7.3^{+4.0}_{-5.9}$	$-8.4^{+4.6}_{-6.6}$
\tilde{s}_2 ($\tilde{s}_1 = 0$)		$-4.1^{+2.3}_{-3.3}$	$-3.2^{+1.8}_{-2.6}$	$-5.7^{+3.1}_{-4.6}$	$-5.2^{+2.9}_{-4.2}$
Case I		206^{+174}_{-115}	269^{+225}_{-152}	271^{+230}_{-151}	321^{+269}_{-180}
Case II		207^{+174}_{-115}	271^{+225}_{-152}	272^{+230}_{-151}	322^{+269}_{-180}

netic spin-orbit interaction, the core polarization effect of the last nucleon, the proton and neutron mass difference in the kinetic energy, and the vacuum polarization, are listed as “Extra” in the Tables V and VI: Each contribution varies from -150 keV to 150 keV, while the net result is at most 100 keV due to a strong cancellation. See Supplemental Material [25] for the details.

The sum of ΔE_{D} , ΔE_{E} and Extra denoted by “Sum (without CSBI)” in the tables is systematically smaller than the experimental value by 3–6%. Our CSBI contributions constrained by the low-energy constants in QCD fill the gap as it can be seen by comparing the sum neglecting CSBI effects, the sum containing CSBI effects “Sum (with CSBI)” and the experimental (“Expt.”) rows in Tables V and VI. Shown in Fig. 2 is $\delta_{\text{ONS}} = \Delta E - \Delta E_{\text{C}}$ where it is evident the agreement between experiment and the present theoretical estimates. The theoretical error bars given in Table IV are shown in the figure, while the experimental error bars are around only 5 keV and would not be visible in the scale of the figure.

Finally, as mentioned, there has been a recent effort in quantifying the effects of CSB in some selected nuclear

TABLE V. The breakdown of the mass differences of mirror nuclei ΔE into each contribution Coulomb, Extra and CSB interaction (CSBI) for Case I with the Skyrme EDF SGII. Numbers are given in units of MeV.

Nuclei	$^{17}\text{F-}^{17}\text{O}$	$^{15}\text{O-}^{15}\text{N}$	$^{41}\text{Sc-}^{41}\text{Ca}$	$^{39}\text{Ca-}^{39}\text{K}$
Orbital	$1d_{5/2}$	$(1p_{1/2})^{-1}$	$1f_{7/2}$	$(1d_{3/2})^{-1}$
ΔE_{D} (Coulomb)	3.596	3.272	7.133	6.717
ΔE_{E} (Coulomb)	-0.203	0.026	-0.267	0.260
Extra	0.040	0.028	0.102	0.011
CSBI (Case I)	0.224	0.264	0.287	0.315
Sum (without CSBI)	3.432	3.326	6.965	6.985
Sum (with CSBI)	3.656	3.590	7.252	7.300
Expt. [36]	3.543	3.537	7.278	7.307

TABLE VI. The same as Table V, but with the Skyrme EDF SAMi.

Nuclei	$^{17}\text{F-}^{17}\text{O}$	$^{15}\text{O-}^{15}\text{N}$	$^{41}\text{Sc-}^{41}\text{Ca}$	$^{39}\text{Ca-}^{39}\text{K}$
Orbital	$1d_{5/2}$	$(1p_{1/2})^{-1}$	$1f_{7/2}$	$(1d_{3/2})^{-1}$
ΔE_{D} (Coulomb)	3.506	3.242	7.025	6.697
ΔE_{E} (Coulomb)	-0.193	0.022	-0.259	0.281
Extra	0.043	0.075	0.104	0.092
CSBI (Case I)	0.206	0.269	0.271	0.321
Sum (without CSBI)	3.356	3.339	6.870	7.070
Sum (with CSBI)	3.562	3.608	7.141	7.391
Expt. [36]	3.543	3.537	7.278	7.307

observables [8, 9, 11, 15, 37]. However, depending on the theoretical method employed, the estimated central values of the leading order term CSB parameter (\tilde{s}_0) can differ by one order of magnitude among the different approaches and could even be of different sign (cf. Ref. [38] and Supplemental Material [25]).

In summary, we evaluated the EDF parameters of Skyrme-type CSB interactions, not only the contact term (\tilde{s}_0) but also the momentum-dependent terms (\tilde{s}_1 , \tilde{s}_2), by utilizing the low-energy constants in QCD and the density dependence of chiral condensation of $\bar{q}q$ pair in the nuclear medium for the first time. The resulting QCD-based CSB interaction is applied to resolve the ONS anomaly: The numerical results for the mirror nuclei ($A = 16 \pm 1$ and $A = 40 \pm 1$ with the isosymmetric core $N = Z = A/2$) with two Skyrme EDFs (SGII and SAMi) show good agreement with experimental data both in sign and magnitude within the theoretical error bars. Major theoretical uncertainty of the final results originates from the values of γ and $\sigma_{\pi N}$: Increasing the accuracy of these constants from the experimental data or from the lattice QCD simulations will be instrumental.

The QCD-based CSB interaction discussed in this Letter would have strong impact on isospin symmetry breaking phenomena such as IAS, the super-allowed β decay in the context of Cabibbo-Kobayashi-Maskawa unitary matrix, and the mass predictions of mirror and isotriplet nuclei near the proton drip line. We plan to make sys-

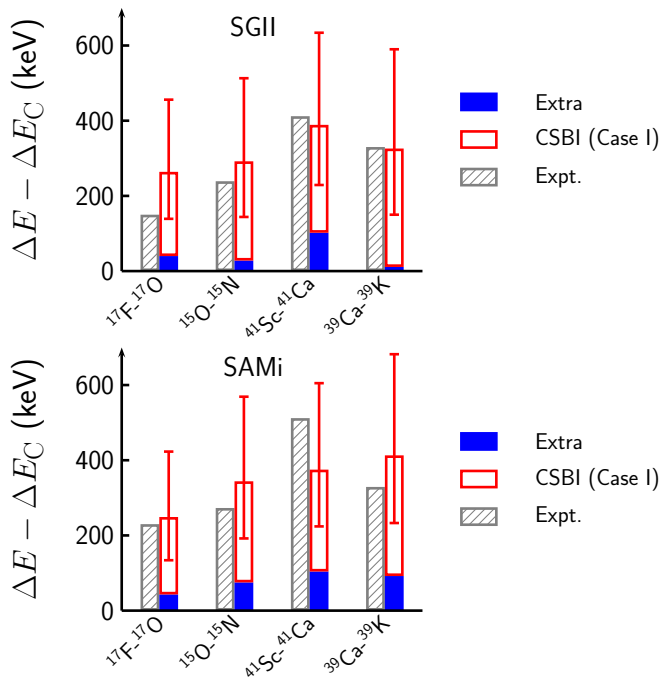


FIG. 2. Comparisons of the experimental ONS anomaly $\Delta E_{\text{Expt.}} - \Delta E_C$ (grey hatched bars) and the corresponding theoretical estimates in two EDFs (SGII and SAMi). The contribution from the QCD-based CSB interaction (CSBI) in Case I and the extra contributions are indicated by the red bars with error bars and the blue bars, respectively.

tematic studies of these quantities.

The authors thank Gianluca Colò and Toshio Suzuki for fruitful discussions. H. S. acknowledges the Grant-in-Aid for Scientific Research (C) under Grant No. 19K03858. T. N. acknowledges the RIKEN Special Postdoctoral Researcher Program, the JSPS Grant-in-Aid for Research Activity Start-up under Grant No. 22K20372, the JSPS Grant-in-Aid for Transformative Research Areas (A) under Grant No. 23H04526, the JSPS Grant-in-Aid for Scientific Research (B) under Grant No. 23H01845, and the JSPS Grant-in-Aid for Scientific Research (C) under Grant No. 23K03426. T. H. was partially supported by JSPS Grant-in-Aid No. 18H05236.

[1] K. Okamoto, Coulomb energy of ^3He and possible charge asymmetry of nuclear forces, Phys. Lett. **11**, 150 (1964).
 [2] J. A. Nolen, Jr. and J. P. Schiffer, Coulomb Energies, Annu. Rev. Nucl. Sci. **19**, 471 (1969).
 [3] S. Shlomo, Nuclear Coulomb energies, Rep. Prog. Phys. **41**, 957 (1978).
 [4] J. W. Negele, The ^{41}Sc - ^{41}Ca Coulomb energy difference, Nucl. Phys. A **165**, 305 (1971).
 [5] P. G. Blunden and M. J. Iqbal, Relativistic Hartree-Fock calculations for finite nuclei, Phys. Lett. B **196**, 295

(1987).
 [6] T. Suzuki, H. Sagawa, and A. Arima, Effects of valence nucleon orbits and charge symmetry breaking interaction on the Nolen-Schiffer anomaly of mirror nuclei, Nucl. Phys. A **536**, 141 (1992).
 [7] G. A. Miller, B. M. K. Nefkens, and I. Slaus, Charge symmetry, quarks and mesons, Phys. Rep. **194**, 1 (1990).
 [8] X. Roca-Maza, G. Colò, and H. Sagawa, Nuclear Symmetry Energy and the Breaking of the Isospin Symmetry: How Do They Reconcile with Each Other?, Phys. Rev. Lett. **120**, 202501 (2018).
 [9] P. Bączyk, J. Dobaczewski, M. Konieczka, W. Satuła, T. Nakatsukasa, and K. Sato, Isospin-symmetry breaking in masses of $N \simeq Z$ nuclei, Phys. Lett. B **778**, 178 (2018).
 [10] H. Sagawa, G. Colò, X. Roca-Maza, and Y. Niu, Collective excitations involving spin and isospin degrees of freedom, Eur. Phys. J. A **55**, 227 (2019).
 [11] P. Bączyk, W. Satuła, J. Dobaczewski, and M. Konieczka, Isobaric multiplet mass equation within nuclear density functional theory, J. Phys. G **46**, 03LT01 (2019).
 [12] T. Naito, G. Colò, H. Liang, X. Roca-Maza, and H. Sagawa, Toward *ab initio* charge symmetry breaking in nuclear energy density functionals, Phys. Rev. C **105**, L021304 (2022).
 [13] T. Naito, X. Roca-Maza, G. Colò, H. Liang, and H. Sagawa, Isospin symmetry breaking in the charge radius difference of mirror nuclei, Phys. Rev. C **106**, L061306 (2022).
 [14] T. Naito, G. Colò, H. Liang, X. Roca-Maza, and H. Sagawa, Effects of Coulomb and isospin symmetry breaking interactions on neutron-skin thickness, Phys. Rev. C **107**, 064302 (2023).
 [15] S. J. Novario, D. Lonardonì, S. Gandolfi, and G. Hagen, Trends of Neutron Skins and Radii of Mirror Nuclei from First Principles, Phys. Rev. Lett. **130**, 032501 (2023).
 [16] R. B. Wiringa, Private communication.
 [17] E. M. Henley and G. Krein, Nambu–Jona-Lasinio model and charge independence, Phys. Rev. Lett. **62**, 2586 (1989).
 [18] T. Hatsuda, H. Høgaasen, and M. Prakash, QCD sum rules in medium and the Okamoto-Nolen-Schiffer anomaly, Phys. Rev. Lett. **66**, 2851 (1991).
 [19] K. Saito and A. W. Thomas, The Nolen-Schiffer anomaly and isospin symmetry breaking in nuclear matter, Phys. Lett. B **335**, 17 (1994).
 [20] Y. Aoki *et al.* (Flavour Lattice Averaging Group (FLAG)), FLAG Review 2021, Eur. Phys. J. C **82**, 869 (2022).
 [21] S. Narison, *QCD as a Theory of Hadrons*, Cambridge Monographs on Particle Physics, Nuclear Physics and Cosmology (Cambridge University Press, Cambridge, 2004).
 [22] R. S. Hayano and T. Hatsuda, Hadron properties in the nuclear medium, Rev. Mod. Phys. **82**, 2949 (2010).
 [23] P. Gubler and D. Satow, Recent progress in QCD condensate evaluations and sum rules, Prog. Part. Nucl. Phys. **106**, 1 (2019).
 [24] S. Goda and D. Jido, Chiral condensate at finite density using the chiral Ward identity, Phys. Rev. C **88**, 065204 (2013).
 [25] See Supplemental Material at [URL will be inserted by publisher] for the fitting procedure of the chiral-condensate as well as the numerical details of various

- contributions to the mass differences of mirror nuclei in the Hartree-Fock calculation [6, 35].
- [26] N. Kaiser, P. de Homont, and W. Weise, In-medium chiral condensate beyond linear density approximation, *Phys. Rev. C* **77**, 025204 (2008).
- [27] J. Gasser, H. Leutwyler, and M. E. Sainio, Sigma term update, *Phys. Lett. B* **253**, 252 (1991).
- [28] T. Nishi, K. Itahashi, D. Ahn, G. P. A. Berg, M. Dozono, D. Etoh, H. Fujioka, N. Fukuda, N. Fukunishi, H. Geissel, E. Haettner, T. Hashimoto, R. S. Hayano, S. Hirezaki, H. Horii, N. Ikeno, N. Inabe, M. Iwasaki, D. Kameda, K. Kisamori, Y. Kiyokawa, T. Kubo, K. Kusaka, M. Matsushita, S. Michimasa, G. Mishima, H. Miya, D. Murai, H. Nagahiro, M. Niikura, N. Nose-Togawa, S. Ota, N. Sakamoto, K. Sekiguchi, Y. Shiokawa, H. Suzuki, K. Suzuki, M. Takaki, H. Takeda, Y. K. Tanaka, T. Uesaka, Y. Wada, A. Watanabe, Y. N. Watanabe, H. Wick, H. Yamakami, Y. Yanagisawa, and K. Yoshida (piAF Collaboration), Chiral symmetry restoration at high matter density observed in pionic atoms, *Nat. Phys.* **19**, 788 (2023).
- [29] H. De Vries, C. W. De Jager, and C. De Vries, Nuclear charge-density-distribution parameters from elastic electron scattering, *At. Data Nucl. Data Tables* **36**, 495 (1987).
- [30] J. Zenihiro *et al.*, Direct determination of the neutron skin thicknesses in $^{40,48}\text{Ca}$ from proton elastic scattering at $E_p = 295$ MeV, arXiv:1810.11796 [nucl-ex] (2018).
- [31] G. Fricke and K. Heilig, Nuclear Charge Radii · 20-Ca Calcium: Datasheet from Landolt-Börnstein - Group I Elementary Particles, Nuclei and Atoms · Volume 20: “Nuclear Charge Radii” in SpringerMaterials (Springer-Verlag Berlin Heidelberg, 2004).
- [32] N. Van Giai and H. Sagawa, Spin-isospin and pairing properties of modified Skyrme interactions, *Phys. Lett. B* **106**, 379 (1981).
- [33] X. Roca-Maza, G. Colò, and H. Sagawa, New Skyrme interaction with improved spin-isospin properties, *Phys. Rev. C* **86**, 031306 (2012).
- [34] E. A. Uehling, Polarization Effects in the Positron Theory, *Phys. Rev.* **48**, 55 (1935).
- [35] N. Van Giai, D. Vautherin, M. Veneroni, and D. M. Brink, Coulomb energy differences in mirror nuclei in the Hartree-Fock approximation, *Phys. Lett. B* **35**, 135 (1971).
- [36] W. J. Huang, M. Wang, F. G. Kondev, G. Audi, and S. Naimi, The AME 2020 atomic mass evaluation (I). Evaluation of input data, and adjustment procedures, *Chin. Phys. C* **45**, 030002 (2021).
- [37] H. Sagawa, S. Yoshida, T. Naito, T. Uesaka, J. Zenihiro, J. Tanaka, and T. Suzuki, Isovector density and isospin impurity in ^{40}Ca , *Phys. Lett. B* **829**, 137072 (2022).
- [38] T. Naito, G. Colò, T. Hatsuda, H. Liang, X. Roca-Maza, and H. Sagawa, Possible inconsistency between phenomenological and theoretical determinations of charge symmetry breaking in nuclear energy density functionals, arXiv:2309.17060 [nucl-th] (2023).

Supplemental Material: QCD-based charge symmetry breaking interaction and Okamoto-Nolen-Schiffer anomaly

Hiroyuki Sagawa (佐川弘幸)^{1,2} Tomoya Naito (内藤智也)^{3,4}
Xavier Roca-Maza^{5,6,7} and Tetsuo Hatsuda (初田哲男)³

¹*RIKEN Nishina Center for Accelerator-based Science, Wako 351-0198, Japan*

²*Center for Mathematics and Physics, University of Aizu, Aizu-Wakamatsu, Fukushima 965-8560, Japan*

³*RIKEN Interdisciplinary Theoretical and Mathematical Sciences Program (iTHEMS), Wako 351-0198, Japan*

⁴*Department of Physics, Graduate School of Science,
The University of Tokyo, Tokyo 113-0033, Japan*

⁵*Departament de Física Quàntica i Astrofísica and Institut de Ciències del Cosmos,
Universitat de Barcelona, Martí i Franqués 1, 08028 Barcelona, Spain*

⁶*Dipartimento di Fisica, Università degli Studi di Milano, Via Celoria 16, 20133 Milano, Italy*

⁷*INFN, Sezione di Milano, Via Celoria 16, 20133 Milano, Italy*

(Dated: January 26, 2024)

In this supplemental material, the fitting procedure of the chiral-condensate as well as the numerical details of various contributions to the mass differences of mirror nuclei in the Hartree-Fock calculation [1, 2] are presented.

IN-MEDIUM CHIRAL CONDENSATE

Figure S.1 shows the next-to-next-to-leading-order (NNLO) chiral condensate in nuclear matter obtained by the in-medium chiral perturbation theory [3];

$$\frac{\langle \bar{q}q \rangle}{\langle \bar{q}q \rangle_0} = 1 - \frac{\sigma_{\pi N}}{f_\pi^2 m_\pi^2} \rho \left(1 - \frac{3k_F^2}{10m_N^2} \right) + \frac{g_A^2 k_F^4}{4f_\pi^4 \pi^4} F \left(\frac{m_\pi^2}{4k_F^2} \right) + \frac{2\sigma_{\pi N}^2 k_F^4}{3f_\pi^4 \pi^4 m_\pi^2} G \left(\frac{m_\pi^2}{4k_F^2} \right), \quad (\text{S.1})$$

with $k_F = (3\pi^2 \rho/2)^{1/3}$ and

$$F(a^2) = \frac{3}{8} - \frac{3}{4}a^2 - \frac{3a}{2} \arctan \frac{1}{a} + \frac{3}{4}a^2 (a^2 + 2) \log \frac{a^2 + 1}{a^2}, \quad (\text{S.2})$$

$$G(a^2) = \frac{3}{8} - \frac{1}{4}a^2 - a \arctan \frac{1}{a} + \frac{1}{4}a^2 (a^2 + 3) \log \left| \frac{1 + a^2}{a^2} \right|. \quad (\text{S.3})$$

Here, we adopt the pion mass $m_\pi = 135$ MeV, the nucleon mass $m_N = 938$ MeV, the nuclear saturation density $\rho_0 = 0.17$ fm⁻³, the pion decay constant $f_\pi = 92.4$ MeV, and the axial-vector coupling constant $g_A = 1.26$. As seen in Fig. S.1, the F - and G -terms originating from the two-loop order are numerically small compared to the whole $\langle \bar{q}q \rangle / \langle \bar{q}q \rangle_0$ at the normal density $\rho = \rho_0$. Hence, we neglect these contributions and consider only the leading-order term with the Fermi motion correction (called in LO* in the main text):

$$\frac{\langle \bar{q}q \rangle}{\langle \bar{q}q \rangle_0} \simeq 1 - \frac{\sigma_{\pi N}}{f_\pi^2 m_\pi^2} \rho \left(1 - \frac{3k_F^2}{10m_N^2} \right). \quad (\text{S.4})$$

In order to check the model dependence on higher-order terms beyond LO*, we consider an alternative calculation of the in-medium chiral condensate, as detailed in Ref. [4]. Shown in Fig. S.2 is a comparison of the LO*, analytic NNLO result in Eq. (S.1) [3] and the numerical result of Ref. [4] with the Δ -excitation. The comparison indicates good agreement among all three cases, especially below ρ_0 . This finding supports the validity of our LO* analysis in the main text.

COULOMB CONTRIBUTIONS TO ΔE IN THE HARTREE-FOCK CALCULATION

The direct term of the Coulomb interaction E_D is calculated by using the valence-proton wave function $\psi_j^p(\mathbf{r})$ of a j -orbital as

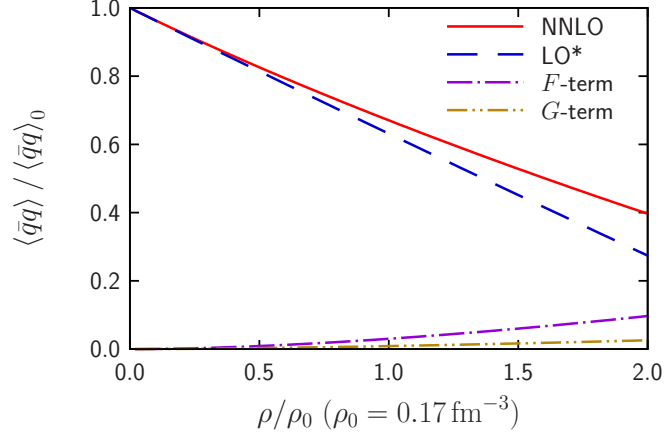


FIG. S.1. The in-medium chiral condensate $\langle \bar{q}q \rangle / \langle \bar{q}q \rangle_0$ obtained by Ref. [3]. The red solid line corresponds to the full NNLO result in Eq. (S.1), while blue long-dashed line corresponds to the result of LO* in Eq. (S.4). The purple dot-dashed line and the yellow dot-dot-dashed line correspond to the F -term and the G -term, respectively.

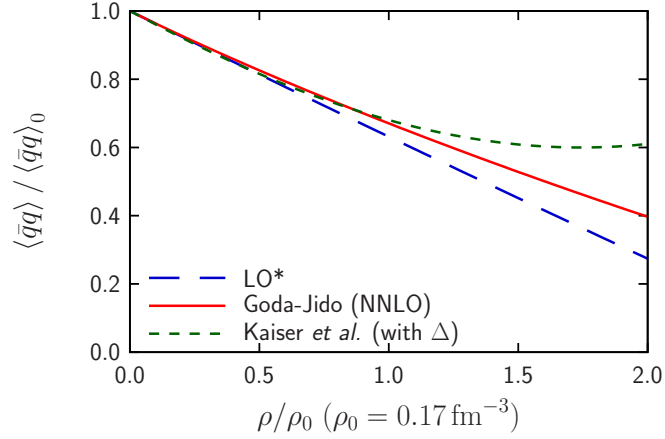


FIG. S.2. The red solid line corresponds to the full NNLO result in Eq. (S.1), while green-dashed line corresponds to the result of Ref. [4] with the Δ -excitation. The blue long-dashed line is the result of LO* in Eq. (S.4). In all three cases, $\sigma_{\pi N} = 45$ MeV is taken.

$$\begin{aligned}
 E_D(j) &= \int V_C(\mathbf{r}) |\psi_j^p(\mathbf{r})|^2 d\mathbf{r} \\
 &= \int d\mathbf{r}'' \int d\mathbf{r}''' \frac{\rho_p(\mathbf{r}''')}{|\mathbf{r}'' - \mathbf{r}'''|} |\psi_j^p(\mathbf{r}'')|^2 \sum_{j' \in \text{core}} \int_0^\infty r^2 dr \int_0^\infty r'^2 dr' R_j^2(r) R_{j'}^2(r') \frac{1}{r_>}, \quad (\text{S.5})
 \end{aligned}$$

where $R_j(r)$ is the radial part of the proton wave function and $r_>$ is the larger of either r or r' . The exact exchange term E_E is given by

$$E_E(j) = - \sum_{j' \in \text{core}} \sum_k (2j' + 1)^{-1} \left\langle j \frac{1}{2} k 0 \middle| j' \frac{1}{2} \right\rangle \int_0^\infty r^2 dr \int_0^\infty r'^2 dr' R_j(r) R_{j'}(r') R_j(r') R_{j'}(r) \frac{r_<^k}{r_>^{k+1}}, \quad (\text{S.6})$$

where $\langle j \frac{1}{2} k 0 | j' \frac{1}{2} \rangle$ is the Clebsch-Gordan coefficient, $r_<$ is the smaller of either r or r' , and the selection rule, $|l_j + k + l_{j'}| = \text{even}$, should be hold. Equation (S.6) is exact in the case $j \neq j'$, i.e., for the particle state. We

take into account the effect of anti-symmetrization properly for the case $j = j'$, which occurs in the calculations of hole states, i.e., we should take care of a factor $1/\sqrt{1 + \delta_{j,j'}}$ for the two-body wave functions, and the direct and exchange contributions are identical for $k = \text{even}$, and cancel for $k = \text{odd}$.

It is important to note that the Coulomb energy depends very much on the radial size of the wave function and, the latter might be different depending on the approach used to obtain it. This is the reason why we compare the r.m.s. radii of our HF calculations with experimental values in Table I of the main manuscript and obtain reasonable agreement (agreement within 0.3%).

EXTRA CONTRIBUTIONS TO ΔE IN THE HARTREE-FOCK (HF) CALCULATION

Finite proton size

The charge distribution of the proton is parametrized by the form factor $f(\mathbf{r}) = \exp(-r^2/a_p^2)/(a_p\sqrt{\pi})^3$. Thus, the charge density is evaluated as

$$\rho_c(\mathbf{r}) = \int d\mathbf{r}' \rho_p(\mathbf{r}') f(\mathbf{r} - \mathbf{r}'). \quad (\text{S.7})$$

Here, we choose $a_p = 0.65$ fm which corresponds to the r.m.s. radius of the proton 0.8 fm, a sufficient accuracy for our purposes.

Center-of-mass effect

The center-of-mass correction is estimated by the harmonic-oscillator model; the HF density is folded by the Gaussian function $g(\mathbf{r}) = \exp(r^2/B^2)/(B\sqrt{\pi})^3$ where $B \equiv b/\sqrt{A} = \sqrt{\hbar/m\omega A}$. The harmonic-oscillator frequency is given by $\hbar\omega = 45/A^{1/3} - 25/A^{2/3}$ MeV. The calculated charge radii obtained from the HF wave functions of the core orbitals reproduce well the empirical ones of ^{16}O and ^{40}Ca in the both parameter sets SGII and SAMi. The calculated charge radii have good agreement with the experimental values within 1% accuracy (see Table III of the main text). This is an important constrain for realistic calculations of Coulomb energy, whose value depends on the charge radii very much.

Thomas-Ehrman effect and isospin impurity

In the mean-field calculations, the proton wave function is different from the neutron one in the same j -orbital because of the Coulomb interaction, i.e., the wave functions of valence protons are calculated by adding the Coulomb interaction to the nuclear interaction adopted for the neutrons in the HF model. This procedure is treated self-consistently in the HF calculations. The self-consistent treatment gives rise to differences between the nuclear potentials for protons and neutrons, i.e., the isospin impurity in the nuclear potential. These effects give rise to the following corrections to the binding energy,

$$\begin{aligned} \delta_{NN}(j) &= \langle \psi_j^p | V_{NN}^p | \psi_j^p \rangle - \langle \psi_j^n | V_{NN}^n | \psi_j^n \rangle \\ &= (\langle \psi_j^p | V_{NN}^n | \psi_j^p \rangle - \langle \psi_j^n | V_{NN}^n | \psi_j^n \rangle) + \langle \psi_j^p | (V_{NN}^p - V_{NN}^n) | \psi_j^p \rangle \\ &\equiv \delta_{NN}^1(j) + \delta_{NN}^2(j), \end{aligned} \quad (\text{S.8})$$

where ψ_j^τ and V_{NN}^τ are the wave function of the j -orbital and the mean-field potential for the nucleon τ ($\tau = p, n$). The term $\delta_{NN}^1(j)$ is due to the difference between the neutron and the proton wave functions of the valence orbital, and is called the Thomas-Ehrman effect. The term $\delta_{NN}^2(j)$ comes from the isospin impurity in the nuclear potential. The correction $\delta_{NN}^1(j)$ appears in all mean-field calculations due to the Coulomb interaction for the protons, while the $\delta_{NN}^2(j)$ term has a contribution only in the self-consistent Hartree or HF calculations.

Electromagnetic spin-orbit interaction

The electromagnetic (EM) spin-orbit interaction is taken into account in the following form:

$$V_{\text{SO}}^{\text{EM}}(\mathbf{r}) = \frac{\hbar^2}{4m^2c^2} \left[(g_p - 1) \left(\frac{1}{2} - t_z \right) + g_n \left(\frac{1}{2} + t_z \right) \right] \times (\mathbf{l} \cdot \boldsymbol{\sigma}) \frac{1}{r} \frac{dV_{\text{C}}(r)}{dr}, \quad (\text{S.9})$$

where $g_p = 5.58$ and $g_n = -3.82$.

Proton-neutron mass difference in the kinetic energy

In the HF calculations, the kinetic energy is evaluated with the average mass of proton and neutron $\bar{m} = (m_p + m_n)/2$. The neutron and proton mass difference, $\Delta m = (m_n - m_p)$, in the proton and neutron kinetic energies in the last orbital is taken into account by the following formula with $\bar{K}^{\text{HF}} = (K_p^{\text{HF}} + K_n^{\text{HF}})/2$ as

$$K_p - K_n \simeq K_p^{\text{HF}} \frac{\bar{m}}{m_p} - K_n^{\text{HF}} \frac{\bar{m}}{m_n} \simeq \bar{K}^{\text{HF}} \frac{\Delta m}{\bar{m}}. \quad (\text{S.10})$$

Core polarization

The core polarization energy caused by the valence nucleon is calculated by performing constrained HF calculations for nuclei with mass $(A_{\text{core}} + 1)$. Namely, the total binding energy $E_{\text{HF}}(A_{\text{core}} + 1)$ is compared with the sum of the binding energy $E_{\text{HF}}(A_{\text{core}})$ and the single-particle energy of the last nucleon $\varepsilon(j)$ calculated in the core potential;

$$\Delta E_{\text{pol}} = E_{\text{HF}}(A_{\text{core}} + 1) - [E_{\text{HF}}(A_{\text{core}}) + \varepsilon(j)]. \quad (\text{S.11})$$

The correction on the energy difference between mirror nuclei is given by

$$\delta_{\text{pol}}(j) = \Delta E_{\text{pol}}^p - \Delta E_{\text{pol}}^n. \quad (\text{S.12})$$

The constrained HF calculations include a spurious self-energy contribution of the last nucleon which should be subtracted. That is, the diagonal two-body matrix element for the last nucleon $E_{\text{spur}}(i) \equiv \frac{1}{2} \langle ii | \bar{V} | ii \rangle$ for $i = A + 1$ is included in the EDF automatically [$\bar{V}(\mathbf{r}_1, \mathbf{r}_2) \equiv V(\mathbf{r}_1, \mathbf{r}_2)(1 - P_{12})$ is the antisymmetrized interaction with P_{12} the exchange operator between nucleons 1 and 2]. This is a spurious matrix element so that it is subtracted from the polarization energy as $E_{\text{pol}} = E_{\text{HF}}(A + 1) - [E_{\text{HF}}(A) + \varepsilon(A + 1)] - E_{\text{spur}}(i)$.

Vacuum polarization

The vacuum polarization effect due to the virtual emission and absorption of electron-positron pairs gives an additional repulsive potential between protons as a lowest order correction in the fine structure constant $\alpha \equiv e^2/\hbar c$ [5]. The corresponding potential induced by the vacuum polarization can be written as [6]

$$V_{\text{VP}}(\mathbf{r}) = \frac{2}{3} \frac{\alpha e^2}{\pi} \int d\mathbf{r}' \frac{\rho_c(\mathbf{r}')}{|\mathbf{r} - \mathbf{r}'|} \mathcal{K}_1 \left(\frac{2}{\lambda_e} |\mathbf{r} - \mathbf{r}'| \right) \quad (\text{S.13})$$

where α is the fine-structure constant, λ_e is the reduced Compton electron wavelength, and

$$\mathcal{K}_1(x) = \int_1^\infty dt e^{-xt} \left(\frac{1}{t^2} + \frac{1}{2t^4} \right) \sqrt{t^2 - 1}. \quad (\text{S.14})$$

The vacuum polarization is estimated to result in a 0.6% increase of the Coulomb energies of both $A = 17$ and 41 systems.

TABLE S.I. Extra contributions to the mass difference of mirror nuclei of $(N \pm 1, Z)$ and $(N, Z \pm 1)$ of $A = N + Z = 16$ and 40 closed shell core. The values are given in units of MeV. The core density and the wave function of valence orbital are calculated by HF model with the SGII Skyrme EDF.

Nuclei	$^{17}\text{F-}^{17}\text{O}$	$^{15}\text{O-}^{15}\text{N}$	$^{41}\text{Sc-}^{41}\text{Ca}$	$^{39}\text{Ca-}^{39}\text{K}$
Orbital	$1d_{5/2}$	$(1p_{1/2})^{-1}$	$1f_{7/2}$	$(1d_{3/2})^{-1}$
Proton size effect	-0.053	-0.070	-0.066	-0.082
Center-of-mass effect	0.023	0.030	0.014	0.018
Thomas-Ehrman effect	0.014	0.006	0.034	0.021
Isospin impurity	0.050	-0.136	0.134	-0.176
EM Spin-orbit interaction	-0.065	0.080	-0.126	0.142
pn mass difference in kinetic energy	0.034	0.024	0.040	0.031
Core polarization	0.018	0.073	0.036	0.020
Vacuum polarization	0.019	0.021	0.036	0.037
Sum	0.040	0.028	0.102	0.011

TABLE S.II. The same as Table S.I, but for the SAMi Skyrme EDF.

Nuclei	$^{17}\text{F-}^{17}\text{O}$	$^{15}\text{O-}^{15}\text{N}$	$^{41}\text{Sc-}^{41}\text{Ca}$	$^{39}\text{Ca-}^{39}\text{K}$
Orbital	$1d_{5/2}$	$(1p_{1/2})^{-1}$	$1f_{7/2}$	$(1d_{3/2})^{-1}$
Proton size effect	-0.050	-0.068	-0.063	-0.080
Center-of-mass effect	0.021	0.029	0.014	0.018
Thomas-Ehrman effect	0.014	0.007	0.031	0.021
Isospin impurity	0.047	-0.090	0.131	-0.098
EM Spin-orbit interaction	-0.061	0.078	-0.121	0.140
pn mass difference in kinetic energy	0.035	0.026	0.041	0.034
Core polarization	0.018	0.073	0.036	0.020
Vacuum polarization	0.019	0.020	0.035	0.037
Sum	0.043	0.075	0.104	0.092

Comparison between different approaches

In Table S.III, we compare the strengths of a Skyrme-like CSB interaction as estimated from different phenomenological ‘‘Pheno’’ [5, 7–9] and microscopic ‘‘Micro’’ [10, 11] approaches. Within the latter, we also show the estimates presented in the main text of the manuscript for an easy comparison. In the phenomenological approaches, a similar Skyrme-like interaction was used; hence, we collect here the published values (accordingly rescaled) while we have used the approach detailed in Ref. [12] to extract, in an approximate way, the equivalent Skyrme-like CSBI parameters of the microscopic calculations of Refs. [10, 11]. As it can be clearly seen from the table, depending on the theoretical method employed, the central values of the leading order term CSB parameter (\tilde{s}_0) can differ by an order of magnitude and could even be of different sign.

TABLE S.III. Strengths of the various Skyrme-like CSB interactions. ‘‘Pheno.’’ and ‘‘Micro.’’, respectively, refer to results based on phenomenological fits and on microscopic evaluation taken from Ref. [13]. See Ref. [13] and text for further details.

Class	Method or Name	\tilde{s}_0 (MeV fm ³)	\tilde{s}_1 (MeV fm ⁵)	\tilde{s}_2 (MeV fm ⁵)	Ref.
Pheno	SAMi-ISB	-52.6 ± 1.4	—	—	[5]
Pheno	SLy4-ISB (leading order)	-22.4 ± 4.4	—	—	[7]
Pheno	SkM*-ISB (leading order)	-22.4 ± 5.6	—	—	[7]
Pheno	SV _T -ISB (leading order)	-29.6 ± 7.6	—	—	[8]
Pheno	SV _T -ISB (next-leading order)	$+44 \pm 8$	-56 ± 16	-31.2 ± 3.2	[8]
Pheno	Estimation by isovector density	-17.6 ± 32.0	—	—	[9]
Micro	ΔE_{tot} (N ² LOGO (394) & CC)	-4.2 ± 6.5	—	—	[10]
Micro	ΔE_{tot} (N ² LOGO (450) & CC)	-5.1 ± 28.5	—	—	[10]
Micro	ΔE_{tot} (AV18-UX & GFMC)	-6.413 ± 0.173	—	—	[11]
Micro	QCD sum rule (Case I)	$-15.5^{+8.8}_{-12.5}$	$+0.52^{+0.42}_{-0.29}$	—	Present
Micro	QCD sum rule (Case II)	$-15.5^{+8.8}_{-12.5}$	—	$+0.18^{+0.14}_{-0.10}$	Present

-
- [1] N. Van Giai, D. Vautherin, M. Veneroni, and D. M. Brink, Coulomb energy differences in mirror nuclei in the Hartree-Fock approximation, *Phys. Lett. B* **35**, 135 (1971).
 - [2] T. Suzuki, H. Sagawa, and A. Arima, Effects of valence nucleon orbits and charge symmetry breaking interaction on the Nolen-Schiffer anomaly of mirror nuclei, *Nucl. Phys. A* **536**, 141 (1992).
 - [3] S. Goda and D. Jido, Chiral condensate at finite density using the chiral Ward identity, *Phys. Rev. C* **88**, 065204 (2013).
 - [4] N. Kaiser, P. de Homont, and W. Weise, In-medium chiral condensate beyond linear density approximation, *Phys. Rev. C* **77**, 025204 (2008).
 - [5] X. Roca-Maza, G. Colò, and H. Sagawa, Nuclear Symmetry Energy and the Breaking of the Isospin Symmetry: How Do They Reconcile with Each Other?, *Phys. Rev. Lett.* **120**, 202501 (2018).
 - [6] E. A. Uehling, Polarization Effects in the Positron Theory, *Phys. Rev.* **48**, 55 (1935).
 - [7] P. Bączyk, J. Dobaczewski, M. Konieczka, W. Satuła, T. Nakatsukasa, and K. Sato, Isospin-symmetry breaking in masses of $N \simeq Z$ nuclei, *Phys. Lett. B* **778**, 178 (2018).
 - [8] P. Bączyk, W. Satuła, J. Dobaczewski, and M. Konieczka, Isobaric multiplet mass equation within nuclear density functional theory, *J. Phys. G* **46**, 03LT01 (2019).
 - [9] H. Sagawa, S. Yoshida, T. Naito, T. Uesaka, J. Zenihiro, J. Tanaka, and T. Suzuki, Isovector density and isospin impurity in ^{40}Ca , *Phys. Lett. B* **829**, 137072 (2022).
 - [10] S. J. Novario, D. Lonardoni, S. Gandolfi, and G. Hagen, Trends of Neutron Skins and Radii of Mirror Nuclei from First Principles, *Phys. Rev. Lett.* **130**, 032501 (2023).
 - [11] R. B. Wiringa, Private communication.
 - [12] T. Naito, G. Colò, H. Liang, X. Roca-Maza, and H. Sagawa, Toward *ab initio* charge symmetry breaking in nuclear energy density functionals, *Phys. Rev. C* **105**, L021304 (2022).
 - [13] T. Naito, G. Colò, T. Hatsuda, H. Liang, X. Roca-Maza, and H. Sagawa, Possible inconsistency between phenomenological and theoretical determinations of charge symmetry breaking in nuclear energy density functionals, arXiv:2309.17060 [nucl-th] (2023).